IJEMS The International Journal for Engineering and Modern Science
Year: 2022 Volume: 1 Issue: 1 Article ID: 22006

Electrical and optical properties of Neodymium ions doped P_2O_5-ZnO-Na_2O-Li_2O glasses

N. F. Osman [1,*], M. E. Sayed [1], M. M. Elokr[2], L. I. Soliman[3], H. A. Zayed[4]

1 Basic Science Department, Modern Academy for Engineering and Technology in Maadi, Cairo, Egypt

2 Physics Department, Faculty of Science, Al-Azhar University, Nasr city, Cairo, Egypt

3 Solid state physics department, Physics Research Institute, National Research Centre, Dokki, Giza

4 Physics Department, Faculty of Women, Ain Shams University, Cairo, Egypt

A R T I C L E I N F O.

Article history:
Received 7 September 2022
Revised 22 October 2022
Accepted 22 October 2022
Available online 24 October 2022

Keywords:
Optical and electrical properties.
Sodium phosphate glasses.
Zinc sodium lithium phosphate glasses.

A B S T R A C T

Sodium zinc lithium phosphate glasses doped with Nd^{3+} were prepared by the melt-quenching method. The optical, structural, and electrical properties of the glass samples were characterized by XRD, density, FTIR and UV-VIS analysis. XRD results revealed that all the samples are amorphous. DTA analysis showed that the transition temperatures of glasses increase with Nd_2O_3 content. FTIR studies revealed that the glasses consist of Q^3, Q^2, Q^1 and Q^0 structural units. The effect of annealing on the absorption coefficient spectra of the samples in the UV-VIS range were studied to evaluate the optical energy gap. The dc, ac electrical conductivity (σ_{dc} and σ_{ac}) and dielectric constants (ε' and ε'') of all the samples have been investigated. Temperature dependence of σ_{dc} is found to obey Arrhenius law. With increasing Nd_2O_3 content σ_{dc} increase while the values of the activation energies ΔE_1 and ΔE_2 decrease. dc conductivity (σ_{dc}) and activation energies (ΔE_1, ΔE_2) were found to be affected by annealing. The ac conductivity follows the power law $\sigma_{ac}(\omega) = A\omega^s$, the exponent s has values between 0.875 and 0.991, consequently the obtained results have been analyzed by (CBH) model. Conductivity mechanisms for grain resistance at room temperature were discussed using the Cole-Cole plot.

1. Introduction

The study of phosphate glasses has attracted much attention because of their applications in high technology. Phosphate glasses possess a series of interesting and unique physical properties better than other glasses such as hardness, transparency at room temperature, sensing laser materials [1], excellent corrosion resistance, low melting temperatures and host for radioactive wastes [2, 3]. For laser application glasses used as transmitting optical components and magneto-optic materials [4].

Lithium contained glasses are broadly used in the industry of electrochemical devices like solid-state batteries, glassy electrolytes, and fuel cells. Optical materials containing Li+ ions can display high conductivity and used as electro-optic switches, modulators, and optical devices [5]. Many studies declared that the physical, structural, and chemical durability of phosphate glasses can be improved by the addition of ZnO because Zn^{2+} ion acts as an ionic crosslinker between different phosphate anions. With the addition of ZnO to phosphate glasses, the P—O—P bonds are replaced by a chemical stronger P—O—Zn bond [6].

*** Corresponding author**
E-mail address: **dr.naglaa_fathy85@yahoo.com (N. F. Osman)**

Therefore, ZnO is an important component for the preparation of multicomponent oxide glasses with low tendency of crystallization [7].

Nowadays, rare-earth doped glasses have been attracting considerable role in the development of low-cost integrated laser sources, sensors, integrated optical amplifier, and photodetectors [8,9] such glasses have potential applications in the area of glass ceramics in electronic devices [10].

This study aims to prepare transparent, bubbles free and stable neodymium-doped P_2O_5-ZnO-Na_2O-Li_2O glassy materials and explain the effect of neodymium doping and annealing temperatures on the structural, optical and electrical properties of(40-x) P_2O_5-20ZnO-25Na_2O-15Li_2O-xNd_2O_3glasses with x = 0.1, 0.4, 0.9, 1.4, 1.9 mol.%.

2. EXPERIMENTAL

2.1. Preparation of the glasses

The investigated glasses (40-x) P_2O_5-20ZnO-25Na_2O-15Li_2O-xNd_2O_3 where, x = 0, 0.1, 0.4, 0.9, 1.4, 1.9 mol.% prepared by the melt quenching technique using high purity analytical grade chemicals $(NH_4)_2HPO_4$, ZnO, Na_2CO_3, LiCl and Nd_2O_3 as raw materials. The appropriate quantity of these chemicals was weighted and mixed in an agate mortar for about one hour. The weighted batches were heated in an electric furnace at 673K for 1/2h in porcelain crucibles to release undesirable gases then melted at 1273K for 1h with intermediate stirring to achieve the homogeneity of the melt. So, samples of the desired shape were obtained by quenching the melt at 623K on a stainless-steel mold for 2h to eliminate the mechanical and thermal stresses produced during casting and left to cooldown at room temperature. The prepared glass samples were polished by silicon carbide waterproof abrasive papers of various grades ranging between 320 and 1000 to achieve good optical transparency sample

2.2. X-ray Diffraction measurements (XRD)

The amorphous nature of synthesized glass samples was checked by PANalytical X'Pert PRO diffractometer using CuKα target of wavelength 1.5406 A° and scanning rate 2 º/min. XRD patterns were recorded in a 2θ range between 4° and 80°.

2.3. Density measurements

The density (ρ) of the glass samples were determined at room temperature by the standard Archimedes method using toluene as an immersion liquid (ρ_t= 0.86455 gm. /cm^3). The density was obtained from the relation,

$$\rho = [W_a / (W_a - W_b)] \cdot \rho_t \quad (1)$$

Where W_a is the weight of the glass sample in air, W_b is the weight of the glass sample when immersed in toluene. The relative error in these measurements was about 1 mg/cm^3. Also, the molar volume (V_m) and the oxygen packing density (OPD) of the glass samples were calculated by using the molecular weight (M) and density (ρ) according to the following relations.

$$Vm = M / \rho \quad (2)$$

$$OPD = 1000 \cdot (\rho / M) \cdot n \quad (3)$$

Where n is the number of oxygen atoms per unit formula.

2.4. Differential Thermal Analysis (DTA)

The glass transition temperature (T_g) and the crystallization temperature (T_C), were evaluated for all the prepared glass samples by using SDT Q600 V20.9 and scanned at a heating rate of 10 °C/min.

2.5. Infrared absorption measurements (FT-IR)

The infrared absorption spectra of the (40-x) P_2O_5-20ZnO-25Na_2O-15Li_2O-xNd_2O_3 glasses were measured at room temperature in the wavenumber range 400-4000 cm^{-1} by a Fourier transform

computerized infrared spectrometer type, JASCO, FT/112 - 43, Japan. The glass samples were prepared by mixing2mg KBr with 200 mg glass powder. Then the weighted mixture was subjected to a pressure of 5 tons/cm^2 to produce clear homogeneous discs. The infrared absorption measurements were measured immediately after preparing the discs.

2.6. Optical band gap

The optical absorption of the glass samples was recorded at room temperature using a double beam Cary 100 spectrophotometer (model UV-12) within the wavelength range 200-900 nm. The uncertainty in the wavelength is found to be ±1 nm.

2.7. Electrical measurements

The prepared samples of the (40-x) P_2O_5-20ZnO-25Na_2O-15Li_2O-xNd_2O_3 glasses were coated with silver paste on both sides for dc and ac electrical conductivity measurements.
The dc and ac electrical conductivity σ for the prepared samples was carried out in the temperature range (303 - 473K). The sample temperature was measured and controlled by using a calibrated Chromel-Alumel thermocouple connected to (TCN4M-24R Aulonics-Korea) temperature controller. For ac electrical conductivity measurements, a programmable automatic LCR bridge (Hioki, 3532-50) was used in a wide frequency range (42Hz to 5MHz).

3. RESULTS AND DISCUSSION

3.1. X- ray Diffraction (XRD)

XRD Patterns of the (40-x) P_2O_5-20ZnO-25Na_2O-15Li_2O-xNd_2O_3 glasses where x = 0, 0.1, 0.4, 0.9, 1.4, 1.9 mol.%are shown in Fig.1(a). The presence of one broad humps in the range of 2θ from 15ºto 40ºconfirming the amorphous nature of the glass. There is no change in the nature of glass (amorphous) after annealing the glass samples for 16 hours at 623K as shown in Fig.1 (b).

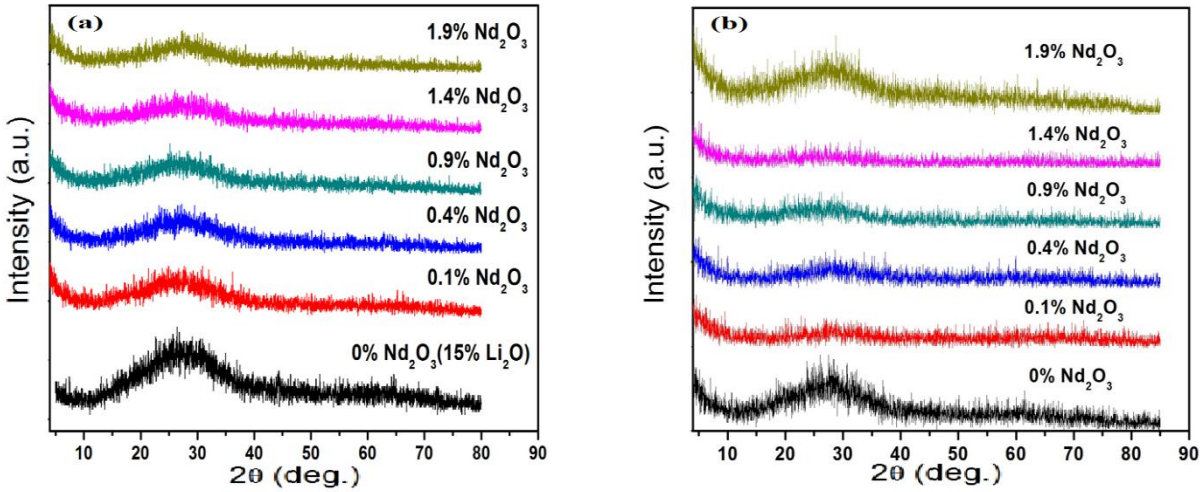

Fig.1. XRD patterns of the (40-x) P_2O_5-20ZnO-25Na_2O-15Li_2O-xNd_2O_3glasses with different concentrations of Nd_2O_3mol.% **(a)** before annealing, **(b)**annealed at 623K for 16h.

3.2. Density measurements

The values of both density (ρ) and molar volume (V_m) for the prepared glass samples with different compositions of Nd_2O_3 before and after annealing at 623K for 16h have been evaluated and their values are given in Table 1. The molecular weight of Nd_2O_3 (336.48 g/mol) is heavier than the molecular weight of the other compounds (the molecular weight of ZnO, P_2O_5, Li_2O andNa_2O are 81.38, 141.94, 29.88, and 61.98 g/mol, respectively) and hence the glass matrix becomes denser when Nd^{3+} ions are introduced as a

dopant into the zinc sodium lithium phosphate glass network [11]. The molar volume (V_m) decreases linearly with increasing the Nd_2O_3 content, this indicates a compact structure with less polymerization due to the shortened chain which confirming that the glass network became well compactable. Oxygen packing density (OPD) is a measure of the tightness of packing of the oxide network which increases linearly with increasing the Nd_2O_3 content as in Table 1, which is an indicator for the increase of the compactness in the glass system.

Neodymium ion concentration (N_{Nd}), polaron radius (r_p), mean inter-ionic distance (r_i) and field strength (F) was calculated by the relations:

Neodymium ion concentration (N_{Nd});

$$N_{Nd} = (\text{ mol.\% of Nd})\, N_A.\rho_g / M_w \quad (4)$$

Polaron radius (r_p);

$$r_p = ½\, (\pi / 6\, N_{Nd})^{1/3} \quad (5)$$

Inter-ionic distance (r_i);

$$r_i = (\, 1 / N_{Nd})^{1/3} \quad (6)$$

Field strength (F);

$$F = Z / r_p^2 \quad (7)$$

Where Z is the ion valency. The calculated values of r_p, r_i and F are given in Table 1. The observed decrease in r_p and r_i with increasing Nd_2O_3 are related to the increased value of Nd-concentrations. This leads to a decrease in Nd–O distance and as a result the Nd–O bond strength increases, producing stronger field strength around Nd^{3+} ions [12].

The electronic polarizability of oxide ions(α_e) is considered to be one of the most important properties of oxide glasses which are related to their applicability in the field of electronics and optics. This can be calculated from the electronegativity of the glass sample.

$$\alpha_e = 4.624 - 0.7569\, \chi_{av} \quad (8)$$

where χ_{av} is the average electronegativity of the compound $\chi_{av} = \sum_{i=1}^{N}(r\, \chi_i n_i / N).(\chi_i)$is Pauling electronegativity [Li=0.98, Na=0.93, O=3.44, P=2.19, Zn=1.65, and Nd=1.14], n_i is no. of atoms in the i^{th} element, N is no. of elements in the compound and r is doping percent).
Theoretical optical basicity (Λ_{th}) of present glasses has been calculated by the following relation:

$$\Lambda_{th} = X_{P2O5}\Lambda_{P2O5} + X_{ZnO}\Lambda_{ZnO} + X_{Na2O}\,\Lambda_{Na2O} + X_{Li2O}\,\Lambda_{Li2O} + X_{Nd2O3}\,\Lambda_{Nd2O3} \quad (9)$$

Where X_{P2O5}, X_{ZnO}, X_{Na2O}, X_{Li2O}, and X_{Nd2O3} are equivalent fractions of P_2O_5, ZnO, Na_2O, Li_2O and Nd_2O_3 based on the amount of oxygen and Λ_{P2O5}, Λ_{ZnO}, Λ_{Na2O}, Λ_{Li2O}, and $\Lambda_{Nd2O3}$are optical basicity values assigned to the individual oxides, respectively. Here the values of $\Lambda_{P2O5} = 0.48$, $\Lambda_{ZnO} = 0.95$, $\Lambda_{Na2O} = 1.15$, $\Lambda_{Li2O} = 1$ and $\Lambda_{Nd2O3} = 1.33$ were obtained from the literature [13, 14]. The obtained values of Λ_{th} are summarized in Table 1. It is observed from Table 1 that the theoretical optical basicity increases with increasing Nd_2O_3 content. The increase in the theoretical optical basicity leads to increase covalency of the cation–oxygen bonds of the studied glasses [15].

Table 1: Density (ρ), molar volume (V_m), oxygen packing density (OPD), Nd^{3+} Ion concentration (N_{Nd}), Polaron radius (r_p), inter ionic distance(r_i), field strength (F), electronic polarizability(α_e) and basicity (Λ_{th}) of the prepared (40-x)P_2O_5-20ZnO-25Na_2O-15Li_2O-xNd_2O_3 glasses ($0 \leq x \leq 1.9$ mol. %).

The composition of Nd_2O_3 (mol.%)	**0**	**0.1**	**0.4**	**0.9**	**1.4**	**1.9**
ρ(g/cm^3)	2.8077	2.9	2.95	2.991	3.01	3.246
V_m (cm^3/mol.)	33.134	32.147	31.8	31.689	31.812	29.8
OPD (g.atom/l)	78.468	80.816	81.51	81.48	80.85	85.976
N_{Nd}(x 10^{21} ions/cm^3)	0	1.873	7.575	17.10	26.50	38.40
r_p (A^o)	0	3.27	2.052	1.56	1.352	1.194
r_i (A^o)	0	8.11	5.092	3.88	3.354	2.964
F (x 10^{16}) (cm^{-2})	0	0.280	0.712	1.23	1.641	2.104
α_e (A$^{o\,3}$)	2.914	3.344	3.350	3.359	3.369	3.379
Λ_{th}(A$^{o\,-3}$)	0.8195	0.8203	0.8229	0.8271	0.8314	0.8356

3.3. Differential Thermal Analysis (DTA)

The variation of DTA curves of the (40-x) P_2O_5-20ZnO-25Na_2O-15Li_2O-xNd_2O_3 glasses where, x = 0, 0.1, 0.4, 0.9, 1.4, 1.9 mol.% are represented in Fig.2. The DTA curves are characterized by an endothermic peak corresponds to glass transition temperature (T_g) and exothermic peak which corresponds to the crystallization temperature (T_C) [16].The non-bridging oxygens disrupt the long chains and break the chemical bonds [2].A parameter (ΔT) was obtained from $\Delta T = T_C - T_g$ which, can be used in the measurements of the glass thermal stability $H' = \Delta T / T_g$ [17, 18]. The characteristic temperatures are calculated and tabulated in Table 2. The value of glass thermal stability H' for the glass sample with Nd_2O_3 content 0.9 mol. % is found to be maximum, which indicates its highest thermal stability than other glasses as represented in the inset of Fig.2.

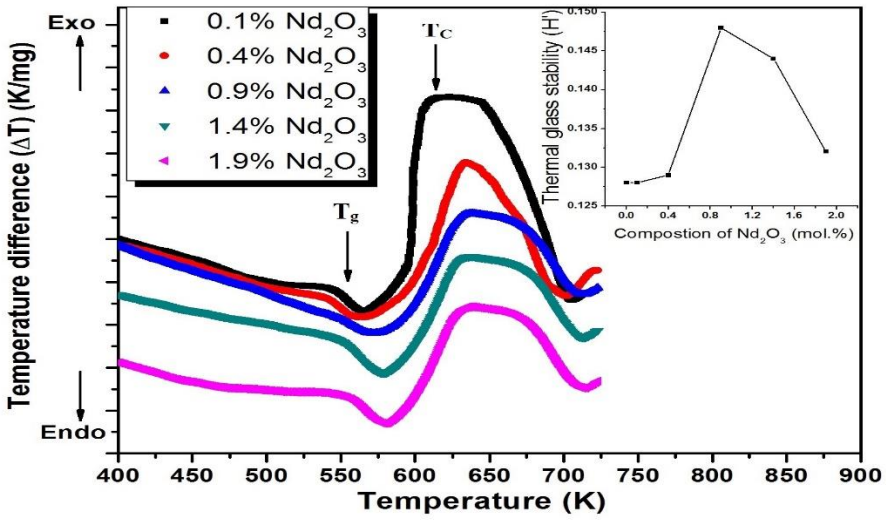

Fig.2 DTA curves of the prepared glass samples with different concentration of Nd_2O_3 mol. %. The inset shows the thermal glass stability (H') for different concentration of Nd_2O_3 mol. %.

Table 2: Thermal constants observed from DTA for the prepared glass samples with different concentration of Nd_2O_3 mol. %.

The composition of Nd_2O_3 (mol. %)	*Glass transition temp.* $T_g(K)$	*Crystallization temp.* $T_C(K)$	$\Delta T = T_c - T_g$ (K)	*Glass thermal stability* $H' = \Delta T / T_g$
0	545.6	615.6	70	0.128
0.1	548	618	70	0.128
0.4	550	631	71	0.129
0.9	553	635	82	0.148
1.4	555	635	80	0.144
1.9	561	635	74	0.132

3.4. Infrared absorption measurements (FTIR)

FTIR spectra of the (40-x) P_2O_5-20ZnO-25Na_2O-15Li_2O-xNd_2O_3 glasses where x = 0, 0.1, 0.4, 0.9, 1.4, 1.9 mol.% in the frequency range of 400-4000 cm^{-1} are shown in Fig.3 and tabulated in Table 3. The FTIR results revealed that the glasses' structure network mainly consists of (O = P—O) in Q^3, (P—O—P) in Q^1 and Q^2, PO_2 in Q^2 and PO_4^{3-} in Q^0. If the modifier content increases in the phosphate matrix, phosphate structural units may be changes from $Q^3 \rightarrow Q^2 \rightarrow Q^1 \rightarrow Q^0$ [19]. The change in structural units from Q^3 to Q^0 provides non-bridging bonds with less polymerization, which forms rigid structures due to the shortened chain length. This observation is confirmed by density and molar volume discussion of the investigated glasses. It is observed also from Fig.3 that bonds of (P—O—P) asymmetric and symmetric stretching modes shift toa higher frequency as the Nd_2O_3 mol.% content increases. This shift can be explained to the increase in the covalent character of (P—O—P) bonds and indicates that (P—O—P) bonds are strengthened as Na_2O and P_2O_5 substituted byNd_2O_3. The shift of these bands at a higher region (525 →542cm^{-1}) and (729 → 741 cm^{-1}), designates the bending vibration of (O=P—O) bonds, and P—O—P symmetric stretching group in the Q^1 structural units respectively [20, 21]. The band between (900→906 cm^{-1}) corresponding to the

asymmetric stretching vibration of (P—O—P) groups in the Q^2 structural unit [22]. Also, the bands (984→ 995 cm^{-1}) and (1102 → 1116 cm^{-1}) are due to symmetric stretching of (PO_4^{3-}) group in the Q^0 structural unit [23]. The asymmetric stretching modes of (PO_2) group in the Q^2 structural unit have appeared in (1286→1289cm^{-1}) [24]. The band 1383 cm^{-1} has appeared in all the Nd_2O_3 doped glass which referred to the stretching mode of P=O [25]. It can be observed that in all glasses these bands(1620 → 1641 cm^{-1}) and (2284 → 2360 cm^{-1}) are due to the bending vibration of H_2O molecules [26,27].A certain shift in the band (3419 → 3470 cm^{-1}) presents in all the investigated glass samples is associated with the oscillations of symmetric stretching of (O—H) group [28].A certain shift in this band at a higher region designates the enhancement of (OH) group.

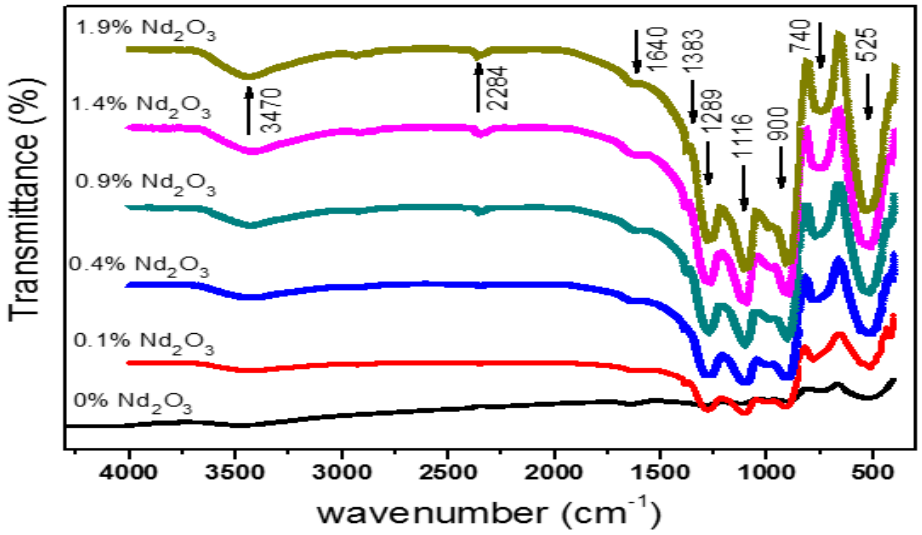

Fig. 3 FTIR spectra of the (40-x) P_2O_5-20ZnO-25Na_2O-15Li_2O- xNd_2O_3 glasses with different concentrations of Nd_2O_3 mol.%.

Table 3: FTIR bands of the (40-x) P_2O_5-20ZnO-25Na_2O-15Li_2O- xNd_2O_3glasses (0 ≤ x ≤ 1.9 mol. %)

Wave numbers (cm^{-1})						***Assignments***
X=0	X=0.1	X=0.4	X=0.9	X=1.4	X=1.9	
525.22	532.69	527.91	528.30	531.35	542.24	Bending vibration of (O=P—O) bond
741.92	734.53	734.54	729.47	730.03	733.85	Symmetric stretching of (P—O—P) group in Q^1 structural unit
900.47	906.62	901.67	904.41	904.51	901.04	Asymmetric stretching of (P—O—P) group in Q^2 structural unit
993.19	995.41	988.52	991.31	987.14	984.01	Symmetric stretching of ($\mathbf{PO_4^{3-}}$)group in Q^0 structural unit
1116.19	1103.06	1100.49	1102.14	1105.39	1102.41	Symmetric stretching of ($\mathbf{PO_4^{3-}}$) group in Q^0 structural unit
1289.60	1273.24	1275.70	1272.02	1268.62	1271.78	Asymmetric stretching of (PO_2) group in Q^2 structural unit
----	1383.68	1383.38	1383.70	1383.82	1383.37	Stretching mode of P=O
1641.72	1631.36	----	1620.54	1632.70	----	Bending vibration H_2O molecule
2284.15	2350.39	2350.41	2360.21	2359.50	2349.28	Bending vibration of (H_2O) molecule
3470.57	3423.41	3440.70	3423.09	3419.62	3431.32	Oscillations due to symmetric stretching of O—H group

3.5. Optical band gap

The optical measurements are productive tools for understanding the band structure and evaluating the bandgap width and optical parameters of disordered materials.

Fig.4 (a, b) show the absorption coefficient before and after annealing for 16h at 623K for the (40-x) P_2O_5-20ZnO-25Na_2O-15Li_2O-xNd_2O_3 glasses where x = 0, 0.1, 0.4, 0.9, 1.4, 1.9mol.%. The absorption coefficient for the glass samples with different concentration has been calculated from this relation [29, 30]:

$$\alpha(\upsilon) = (1/t).\ln(\frac{1}{T}) = (1/t).\ln A \quad (10)$$

Where T is the transmittance, t is the thickness of the glass sample, and A is the absorbance.

The absorption coefficient for these glasses(40-x) P_2O_5-20ZnO-25Na_2O-15Li_2O-xNd_2O_3 is related to the photon energy (hυ) which is given by the relation:

$$\alpha(\upsilon) = \text{const.}\,.\,(h\upsilon - E_g)^n \,/\, h\upsilon \quad (11)$$

where the const. is dependent on the transition probability, E_g is the width of the bandgap and n is an index that characterizes the optical absorption processes in all investigated glasses and is equal to 2, 1/2, 3, 3/2 for an indirect allowed, direct allowed, indirect forbidden, and direct forbidden transition respectively [31]. For the amorphous material, the transition processes are usually corresponding to the indirect transition therefore, the optical band gap (E_g) can be determined by extrapolating the linear part of curve to the hυ axis where$(\alpha h\upsilon)^{1/2}=0$ as shown in Fig.5(a, b) before and after annealing for the (40-x) P_2O_5-20ZnO-25Na_2O-15Li_2O-xNd_2O_3 glasses. So, the optical band gap energy was calculated for such glasses by linear fitting of the high absorption regions. The intersection on hυ-axis corresponded to the optical band gap E_g with $(\alpha h\upsilon)^{1/2}$ equals zero.

In the present study, the energy gap can be presented as in the inset of Fig.5 (a, b) for different compositions of Nd_2O_3 where, x=0, 0.1, 0.4, 0.9,1.4, 1.9 mol.%. It is found that the energy gap E_g decreases from 3.217 to 2.66 eV before annealing and decreases from 2.72 to 2.33 eV after annealing by increasing Nd_2O_3 content.

The refractive index (n) is considered to be one of the most important optical parameters of materials which is related to the electronic polarizability of ions and the local field of the material [32]. The refractive index is related to the optical bandgap of the glass through the following:

$$[(n^2 -1) / (n^2+2)] = 1- \sqrt{E_g/20} \quad (12)$$

The increasing values of the refractive index with increasing Nd_2O_3content are understood in terms of the formation of NBO in the glass matrix [33]. This means that the presence of Nd_2O_3 in glass can act as a glass modifier and lead to increase NBO bonds inside the glass matrix.

The metallization criterion, M, can be used for predicting metallic or insulating behavior in the solid-state material and is given by [34]:

$$M = 1 – [(n^2 -1) / (n^2 +2)] \quad (13)$$

Where n is the refractive index, the values of M are listed in Table 4. It is found that the present glasses exhibit an insulating nature.

The optical conductivity is most conveniently studied to indicate the optical response of a material. The optical conductivity (σ_{opt}) has been determined from the relation [35] $\sigma_{opt} = \alpha nc/4\pi$, where c is the velocity of light, α is the absorption coefficient n is the refractive index. Fig. 6 shows the plot of optical conductivity versus wavelength before and after annealing for the prepared glass samples. The optical conductivity directly depends on the absorption coefficient, and the refractive index of the material and it has the same trend as that of the absorption coefficient with increasing wavelength.

Table 4: energy gap (E_g), refractive index (n) and metallization criterion (M) before and after annealing of the prepared (40-x) P_2O_5-20ZnO-25Na_2O-15Li_2O- xNd_2O_3glasses ($0 \leq x \leq 1.9$ mol. %).

Composition of Nd_2O_3 (mol.%)	**0**	**0.1**	**0.4**	**0.9**	**1.4**	**1.9**
Before annealing						
E_g (eV)	3.217	3.14	3.04	2.85	2.77	2.66
N	2.341	2.361	2.386	2.436	2.463	2.494
M	0.401	0.396	0.390	0.370	0.372	0.365
After annealing (16 hours at 623K)						
E_g (eV)	2.72	2.64	2.61	2.50	2.36	2.33
N	2.476	2.503	2.512	2.544	2.592	2.607
M	0.369	0.363	0.361	0.354	0.344	0.341

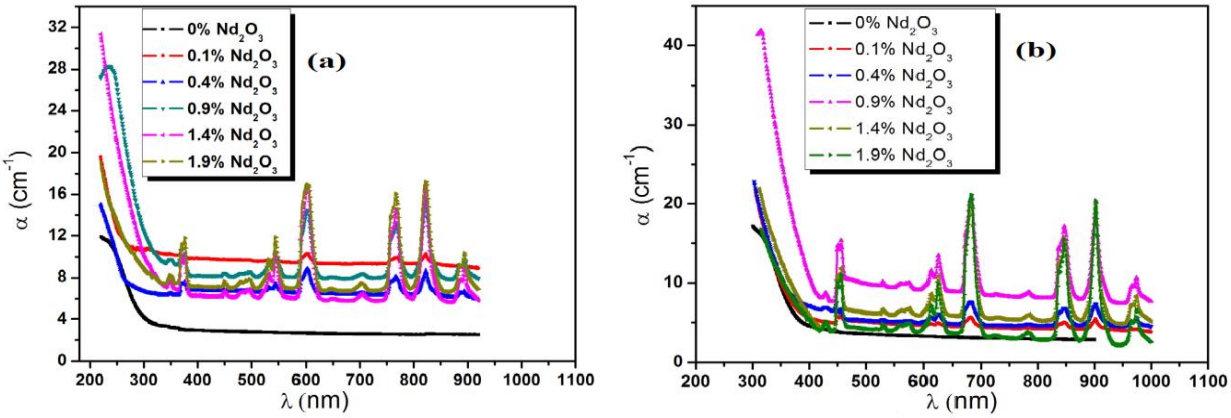

Fig. 4 Absorption coefficient spectra of the (40-x) P_2O_5-20ZnO-25Na_2O-15Li_2O- xNd_2O_3 glasses with different concentrations of Nd_2O_3 mol. %**(a)** before annealing and **(b)** after annealing for 16 hours at 623K.

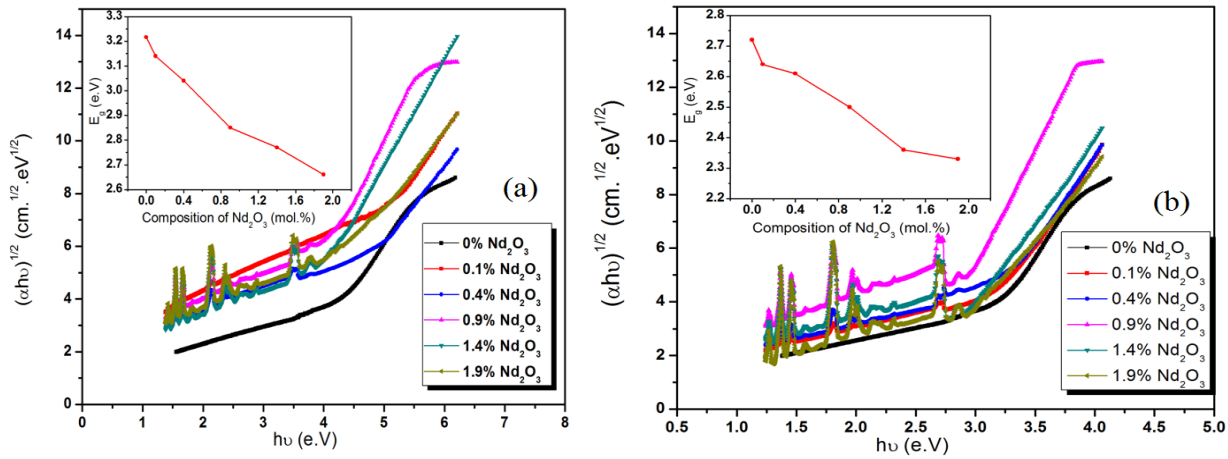

Fig. 5: Variation of $(\alpha h\upsilon)^{1/2}$with hυ (eV) for the (40-x) P_2O_5-20ZnO-25Na_2O-15Li_2O- xNd_2O_3 glasses with different concentrations of Nd_2O_3mol %**(a,b)** before and after annealing for 16 hours at 623K. The inset shows the variation of E_g (eV) with the concentration of Nd_2O_3mol %.

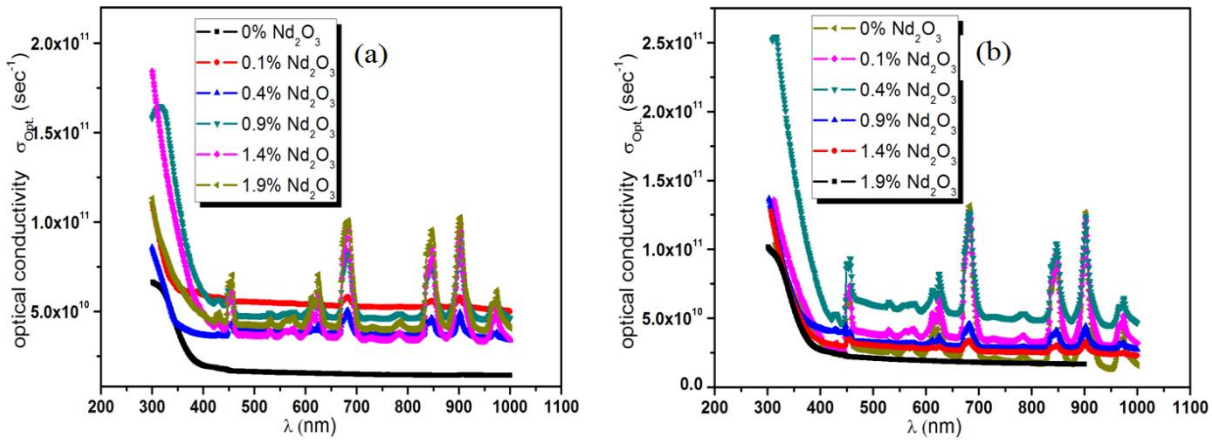

Fig. 6 Variation of optical conductivity $\sigma_{opt.}$ (sec^{-1}) with λ (nm) for the (40-x) P_2O_5-20ZnO-25Na_2O-15Li_2O- x Nd_2O_3 glasses with different concentrations of Nd_2O_3 mol. %**(a, b)** before and after annealing for 16 hours at 623K.

3.6. Electrical conductivity

3.6.1. DC electrical conductivity

The temperature dependence of dc electrical conductivity of the (40-x) P_2O_5-20ZnO-25Na_2O-15Li_2O-xNd_2O_3 glasses where, x = 0, 0.1, 0.4, 0.9, 1.4, 1.9 mol.% before annealing are shown in Fig.7 (a). The data fit the Arrhenius equation:

$$\sigma_{dc} = \sigma_o \exp(-E_a / kT), \quad (14)$$

σ_o is the pre-exponential factor which including the charge carrier mobility and density of states, E_a is the thermal activation energy for conduction and k is the Boltzmann constant. There are two linear regions of conductivity that gave two activation energies ΔE_{dc1} for high temperatures (403-473K) region and ΔE_{dc2} for low temperatures (303-383K) region which arise from impurity scattering.

The variation of σ_{dc} at room temperature and the activation energies ΔE_{dc1} and ΔE_{dc2} with the concentration of Nd_2O_3 (mol. %) before annealing are represented in the inset of Fig.7 (a). It is clear from the inset of Fig.7 (a) that σ_{dc} increases from $1.027x10^{-5}$ to $1.67x10^{-5}$ ($\Omega^{-1}.cm^{-1}$) with increasing of Nd_2O_3 content. The phosphorus ions were gradually replaced by neodymium ions because the amount of glass former Na_2O was fixed at 25 mol.%, Li_2O was fixed at 15 mol.% and glass modifier ZnO was fixed at 20 mol.%. Such behavior is likely to arise due to structural changes occurring in the phosphate network. The activation energies ΔE_{dc1} and ΔE_{dc2}calculated from analysis of Ln σ_{dc} versus 1000 / T plots are found to decrease with increasing Nd_2O_3 content.

After annealing, the variation of σ_{dc} at room temperature and the activation energies ΔE_{dc1} and ΔE_{dc2} with the concentration of Nd_2O_3 (mol. %) are represented in the inset of Fig.7 (b). So, σ_{dc} increases from $1.29x10^{-5}$ to $2.49x10^{-5}$ ($\Omega^{-1}.cm^{-1}$) with increasing of Nd_2O_3 content. Also, the activation energies calculated from analysis of Ln σ_{dc} versus 1000 / T plots are found to decrease with increasing Nd_2O_3 content.

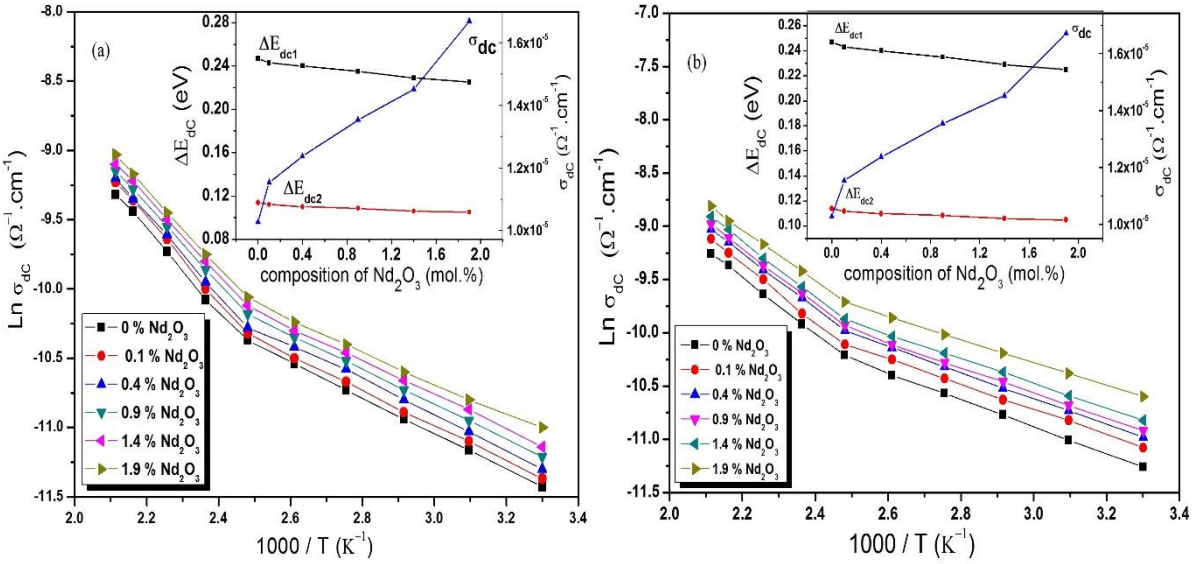

Fig. 7:(a) Variation of Ln σ_{dc} with1000/T and the inset shows the Variation of ΔE_{dc} and σ_{dc} for different concentration of Nd_2O_3 before annealing. **(b)**Variation of Ln σ_{dc} with 1000/T and the inset shows the Variation of ΔE_{dc} and σ_{dc} for different concentration of Nd_2O_3 after annealing for 16 hours at 623k.

3.6.2. Complex impedance analysis

Complex impedance is a powerful technique for the characterization of electrical properties of polycrystalline samples such as conductivity, dielectric behavior …. etc. It may be used to explain the dynamics of mobile or bound charges in the grain or grain boundaries. The expression of real (Z') and imaginary (Z") components of the impedance (Z) can be expressed by the following relationships:

$$Z = Z' - jZ'' \quad (15)$$

$$Z' = Z \cos Q \quad (16)$$

$$Z'' = Z \sin Q \quad (17)$$

Where $Q = 1 / [C.Z.(2\Pi f)]$

Fig. 8 shows the plot of Z' versus Z" (Cole-Cole plot) for the prepared glass samples with different compositions of Nd_2O_3 at constant temperature (423K) (a) before annealing, (b) after annealing for 16 hours at 623K. Fig. 9 shows the plot of Z' versus Z" (Cole-Cole plot) for the prepared glass samples with different temperatures at constant composition (0.1 mol. % of Nd_2O_3) (a) before annealing, (b) after annealing for 16 hours at 623K. The impedance plots of all the samples were found to exhibit a good single semicircle starting from the origin over the entire range of temperature and the composition studied. The absence of the second semicircle in the complex impedance plots indicates that the glass samples have only a grain effect on the conductivity mechanism at room temperature. The values of dc conductivity were calculated by taking the intersection points of semicircles on the Z' axis [36]. Figures 8, 9(a) illustrated that the diameter of the semicircle decreasing, and the intersection points of the semicircles shifted to lower Z' values with increasing temperature and with increasing Nd_2O_3 content in glass samples which suggests that the value of grain resistance is decreasing and σ_{dc} increasing with increasing temperatures and the value of grain resistance is decreasing to minimum.

After annealing, Figures 8, 9 (b) illustrated that the annealing cause the diameter of the semicircle decreasing again and the intersection points of the semicircles shifted to lower Z' values with increasing temperature and with increasing Nd_2O_3 content in glass samples.

To compare the obtained data of σ_{dc} calculated from Cole-Cole and σ_{dc} calculated from σ_t versus frequency are listed in Table 5. It is clear that σ_{dc} (Cole-Cole) and σ_{dc} (σ_t vs. f) approximately have the same values.

Table 5: values of σ_{dc} (Cole-Cole) and σ_{dc} (σ_t vs. f) at different temperatures (for constant concentration 0.1% Nd_2O_3 mol. %) before and after annealing.

Temperature T (K)	**403**	**423**	**443**	**463**	**473**
Before annealing					
σ_{dc} (Cole-Cole)	$3.1 * 10^{-5}$	$4.43 * 10^{-5}$	$6.66 * 10^{-5}$	$8.45 * 10^{-5}$	$9.73 * 10^{-5}$
σ_{dc} (σ_t Vs f)	$3.30 * 10^{-5}$	$4.54 * 10^{-5}$	$6.87 * 10^{-5}$	$8.6 * 10^{-5}$	$9.80 * 10^{-5}$
After annealing (16 hours at 623K)					
σ_{dc} (Cole-Cole)	$3.94 * 10^{-5}$	$5.42 * 10^{-5}$	$7.30 * 10^{-5}$	$9.58 * 10^{-5}$	$1.11 * 10^{-5}$
σ_{dc} (σ_t Vs f)	$4.07 * 10^{-5}$	$5.43 * 10^{-5}$	$7.48 * 10^{-5}$	$9.61 * 10^{-5}$	$1.09 * 10^{-5}$

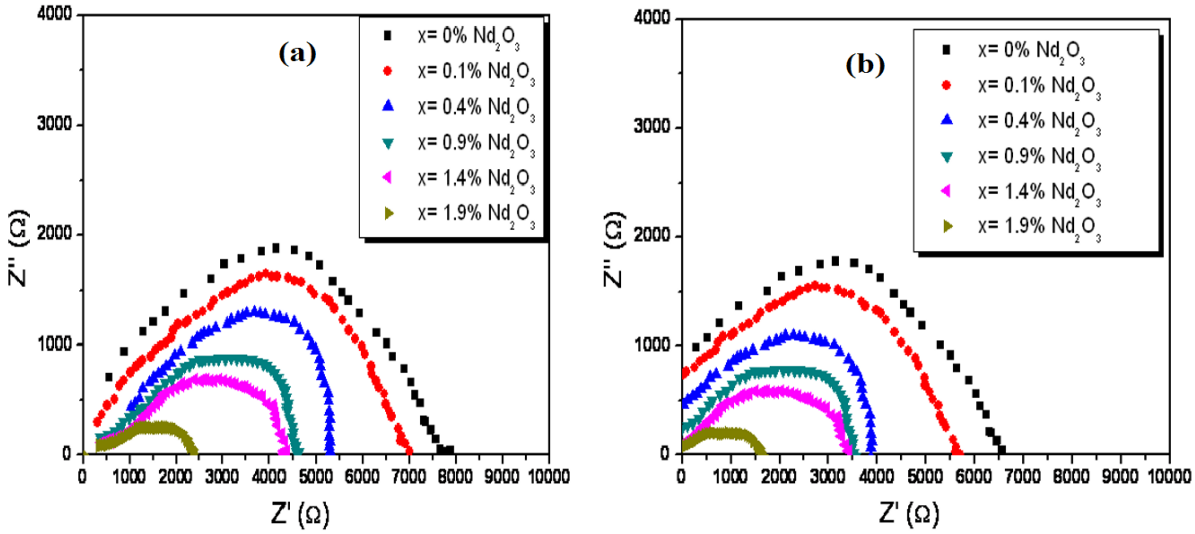

Fig. 8: Cole-Cole plots for glass samples with different concentration of Nd_2O_3at constant temperature 423 K **(a)** before annealing and **(b)** after annealing for 16 hours at 623k.

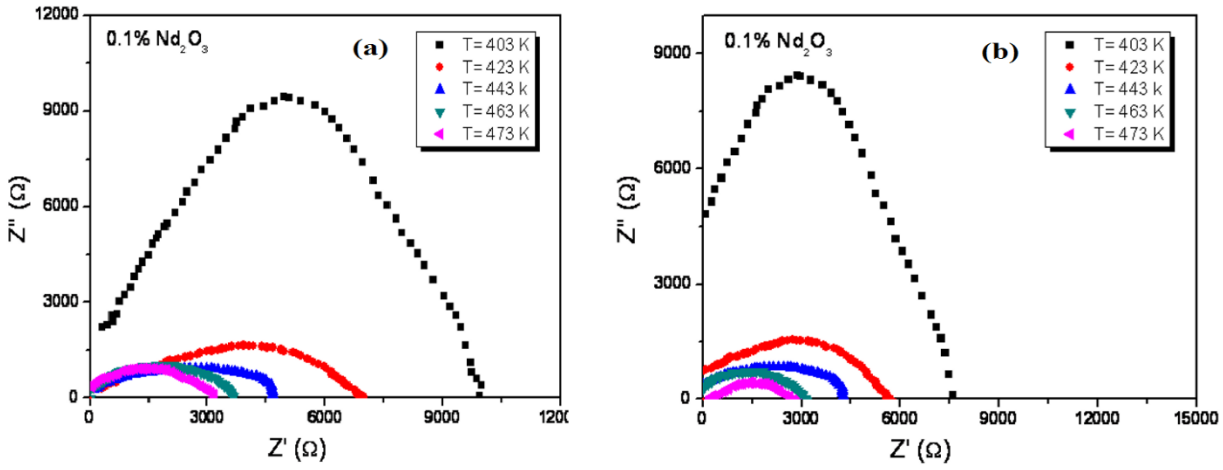

Fig. 9: Cole-Cole plots of Z' and Z" for glass sample containing0.1% Nd_2O_3 (mol. %) at different temperatures **(a)** before annealing and **(b)** after annealing for 16 hours at 623k.

3.6.3. AC electrical conductivity

The ac conductivity σ_{ac} can be described by Eqn. (18) Where, σ_t is the total conductivity and σ_{dc} is the dc conductivity at zero frequency ($\omega = 0$). At very low-frequency region σ_{dc} is independent of frequency and appears as a flat dc plateau in this region of frequency. The ac conductivity is approximately independent of the frequency at lower frequencies, but more frequency-dependent in high-frequency region. The ac conductivity follows the relation:

$$\sigma_{ac}(\omega) = \sigma_t - \sigma_{dc}(\omega = 0) \quad (18)$$

In this relation, the dc conductivity is taken to represent the ac conductivity at ω tends to zero. The ac conductivity has been analyzed used Almond-West type power-law with a single exponent [37].

$$\sigma_{ac} = A \cdot \omega^s \quad (19)$$

Where A is a temperature-dependent constant, $\omega = 2\pi f$ is the angular frequency and s is the frequency exponent which is temperature dependent. Such a dependence on temperature determines the ac conduction mechanism that depend on material.

3.6.4. Frequency and temperature dependence of ac electrical conductivity

Fig.10 (a)shows the frequency dependence of ac electrical conductivity at different temperatures for the (40-x) P_2O_5-20ZnO-25Na_2O-15Li_2O-xNd_2O_3glasses (with x = 1.4mol. % Nd_2O_3) before annealing. The ac conductivity behavior of all the other glass samples (with x = 0, 0.1,0.4, 0.9, 1.9 mol. % Nd_2O_3) is qualitatively similar.

The increase of σ_{ac} with increasing frequency suggests that hoping conduction prevails and the increase of the applied frequency enhances the hopping of charge carriers between the localized states [38]. Also, the annealing improving the increase in σ_{ac} as illustrated in Fig. 10 (c).

The values of the exponent s (Eqn.19) were calculated from the slopes of these lines at different temperatures. The temperature dependence of s for all the prepared glass samples with different concentrations before annealing is shown in Fig.10 (b) in which s decreases with increasing temperature and the concentration of the Nd_2O_3.Also, it was found that for all the prepared glass samples s values are significantly lower than unity and lie between 0.878-0.991. After annealing, the values of the exponent s were also calculated and had values lie between 0.875-0.990 which is lower than those values calculated before annealing as shown in Fig. 10 (d).

According to correlated barrier hopping (CBH) model values of s decrease with increasing temperatures which is in good agreement with the obtained results shown in Fig.10 (b, d). Accordingly, the frequency dependence of σ_{ac} can be explained in terms of the CBH model. This model first developed by Pike [39] for single-electron hopping and has been extended by Elliot and Chen [40, 41] for simultaneous two-electron hopping. Fig.11 (a, b) shows the variation of Ln σ_{ac} with the reciprocal of temperature 1000 / T in the investigated temperature range at different frequencies for the (40-x) P_2O_5-20ZnO-25Na_2O-15Li_2O-xNd_2O_3 glasses (with x = 1.4mol. % Nd_2O_3) before and after annealing. This dependence of ac conductivity on temperature suggests that the ac conductivity is a thermally activated process. The value of the activation energies ΔE_{ac} has been calculated from the slope of Ln σ_{ac} versus 1000 / T curves.

Fig.11 (c, d) shows the variation of the activation energies ΔE_{ac} with the concentration of Nd_2O_3 mol. % at different frequencies before and after annealing. It is found that the activation energies ΔE_{ac} decrease with an increase of Nd_2O_3 concentration [42].

The variation of ac activation energies ΔE_{dc} and σ_{dc} with the concentration Nd_2O_3 mol.% at constant frequency (3MHz) and at room temperature before and after annealing was illustrated in Table 6.

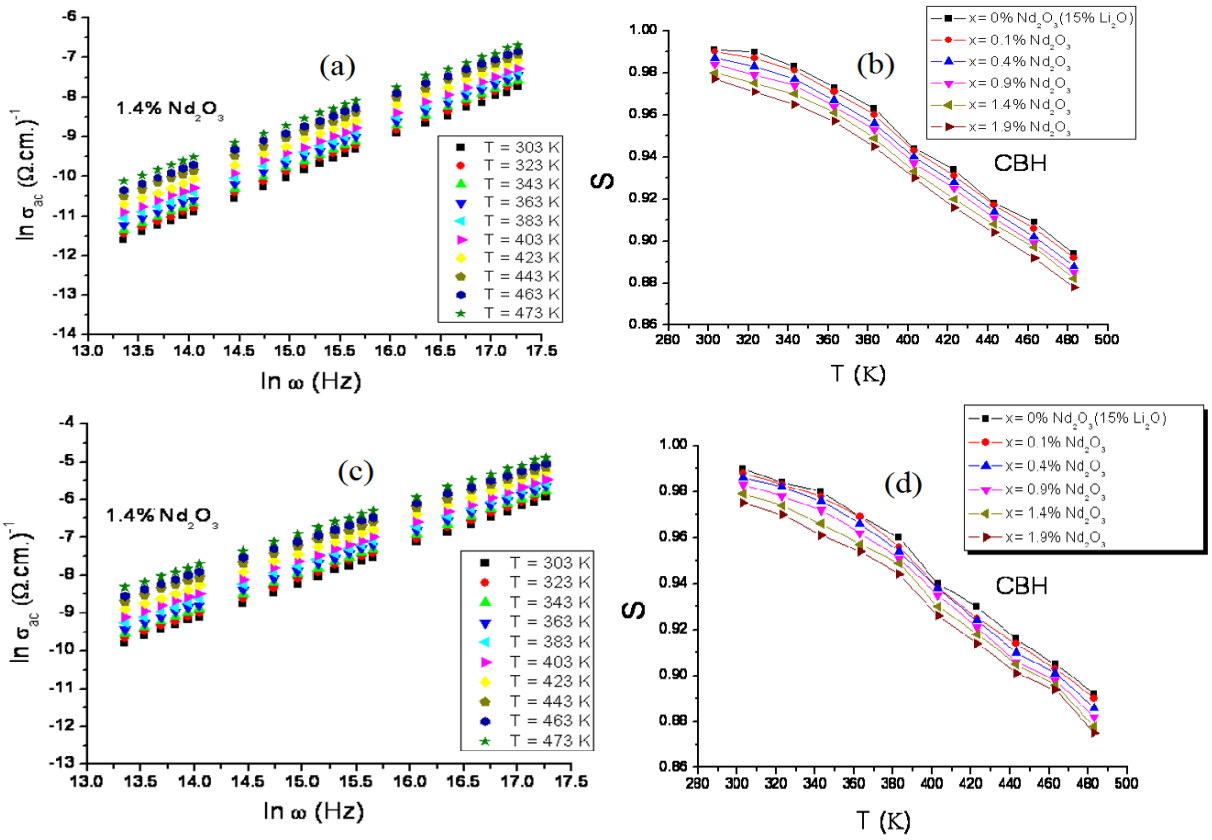

Fig. 10: Frequency dependence of σ_{ac} for glass containing 1.4mol.% Nd_2O_3 at different temperatures **(a, c)** before and after annealing for 16 hours at 623k and temperature dependence of the frequency exponent (s) at different concentrations ofNd_2O_3 (mol. %) **(b, d)** before and after annealing for 16 hours at 623k.

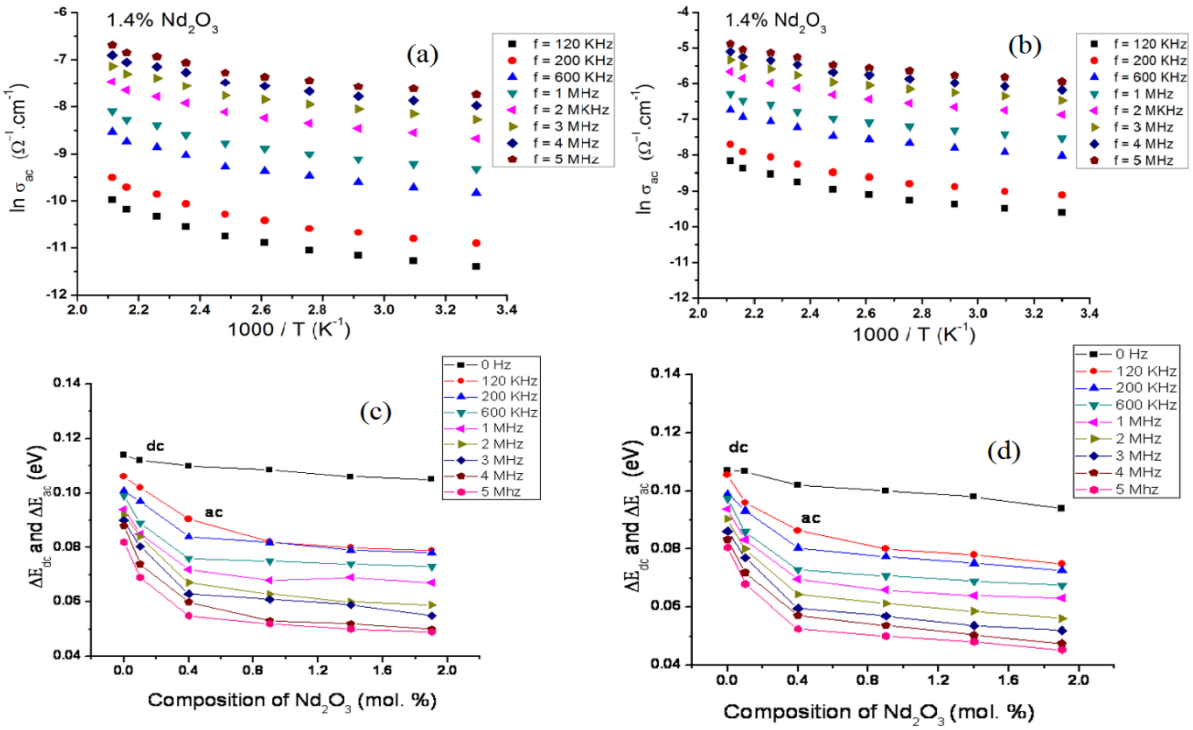

Fig. 11: Temperature dependence of ac conductivity for glasses 1.4 mol.% of Nd_2O_3 at different frequencies **(a, b)** before and after annealing for 16 hours at 623K and the variation of ac activation energies ΔE_{ac} and ΔE_{ac} with the concentration of Nd_2O_3mol.% at different frequencies **(c, d)** before and after annealing for 16 hours at 623k.

Table 6: Values of σ_{ac} and ΔE_{ac} with different concentrations ofNd_2O_3 (mol.%) before and after annealing at constant frequency (3 MHz) and at room temperature.

Composition of Nd_2O_3 (mol.%)	**0**	**0.1**	**0.4**	**0.9**	**1.4**	**1.9**
Before annealing						
σ_{ac} **(Ω.cm)$^{-1}$**	$8.73 * 10^{-5}$	$1.350 * 10^{-4}$	$1.656* 10^{-4}$	$2.442* 10^{-4}$	$2.56 * 10^{-4}$	$2.622 * 10^{-4}$
ΔE_{ac} **(eV)**	0.090	0.0805	0.063	0.061	0.059	0.055
After annealing (16 hours at 623K)						
σ_{ac} **(Ω.cm)$^{-1}$**	$2.31 * 10^{-4}$	$4.174 * 10^{-4}$	$6.715 * 10^{-4}$	$1.209 * 10^{-3}$	$1.55 * 10^{-3}$	$1.94 * 10^{-3}$
ΔE_{ac} **(eV)**	0.0862	0.077	0.0596	0.057	0.0537	0.052

3.6.5. Temperature and frequency dependence of dielectric constant ε' and ε''

The complex dielectric constant of the investigated samples is formulated with two parts, $\varepsilon = \varepsilon' + i\,\varepsilon''$; where ε' is the real part of dielectric constant and it is a measure of the energy, stored from the applied electric field in the material and identified the strength of alignment of dipoles in the dielectric. ε'' is the imaginary part of dielectric constant and it is the energy dissipated in the dielectric. ε' and ε'' were evaluated using the following relations:

$$\varepsilon' = C\,L / \varepsilon_o A \tag{20}$$

$$\varepsilon'' = \varepsilon' \tan\delta \tag{21}$$

Where C is the capacitance of the sample, ε_o is the free space permittivity, L is the sample thickness and A is the area and tan δ is the dissipation factor.

The imaginary part of dielectric constant ε'' of (40-x) P_2O_5-20ZnO-25Na_2O-15Li_2O-xNd_2O_3 glasses (with x = 1.4mol. % Nd_2O_3) before and after annealing samples with different concentration of Nd_2O_3 are measured over the frequency range from 50 Hz to 5 MHz as shown in Fig.12 (a, b).

According to Guntini et al [43] ε'' at a particular frequency in the temperature range where dielectric dispersion occurs, is given by:

$$\varepsilon'' = B\,\omega^m \tag{22}$$

The power m of this equation was calculated from the negative slopes of the straight lines at different temperatures before and after annealing. The variation of the obtained values of m with temperature for different concentrations of Nd_2O_3 before and after annealing is shown in Fig.12 (c, d). According to Guintini et al, the exponent m can be related to the temperature and the maximum barrier height W_m through the following equation:

$$m = -4K_BT/W_m \tag{23}$$

It is found that the maximum barrier height W_m is decreased with increasing concentration and annealing which are tabulated in Table 7.

Table 7: Maximum barrier height (W_m) for the (40-x)P_2O_5-20ZnO-25Na_2O-15Li_2O- xNd_2O_3glasses ($0 \leq x \leq 1.9$ mol. %).

The glass composition (mol.%)	*Maximum barrier height (W_m) (Before annealing)*	*Maximum barrier height (W_m) (After annealing)*
0	**0.112**	**0.1094**
0.1	**0.108**	**0.1058**
0.4	**0.107**	**0.1032**
0.9	**0.106**	**0.101**
1.4	**0.105**	**0.0997**
1.9	**0.1038**	**0.0982**

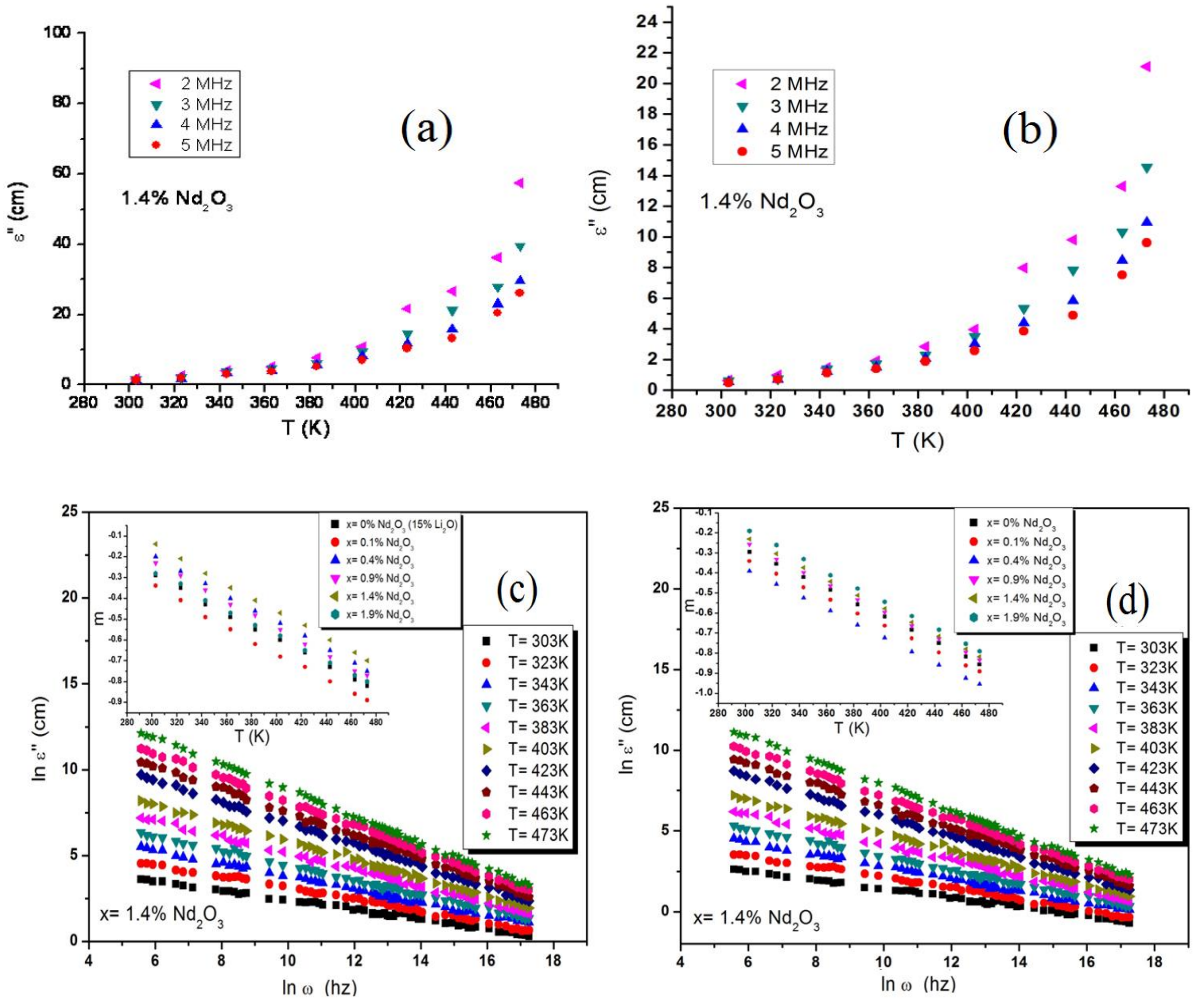

Fig. 12: The temperature dependence of imaginary part (ε") of glass containing 1.4 mol.%Nd_2O_3at different frequencies **(a,b)** before and after annealing and the temperature dependence of ln ε" with ln ω for different temperatures**(c, d)** before and after annealing. The insets of **Fig. 12**showthetemperature dependence of the exponent (m) for the investigated glassesat different concentrations ofNd_2O_3 mol. % **(c)**before and **(d)**after annealing for 16 hours at 623k.

4. Conclusions

Nd_2O_3 doped zinc sodium lithium phosphate glass samples were prepared by the conventional melt quenching technique. The amorphous nature of the prepared glasses was confirmed by XRD patterns. By increasing the Nd_2O_3 content mol.% the density of the glass samples was found to be increasing due to the larger molecular weight of Nd_2O_3 (336.48 g/mol.) compared with the other oxides in the glass matrix. FTIR studies revealed that the glasses consist of Q^3, Q^2, Q^1 and Q^0 structural units. The indirect optical energy gaps were evaluated from UV-VIS absorption spectra and were found to be decreasing with increasing Nd_2O_3 content mol.% and annealing temperature. The temperature dependence of dc conductivity was found to obeys Arrhenius law and increase with increasing Nd_2O_3 content mol.% and the ac conductivity obeys the power law $\sigma_{ac}(\omega) = A(T)\ \omega^{S(T)}$, where s<1. The (CBH) model seems to be the most interesting model to discuss the obtained results. Conductivity mechanisms for grain resistance at room temperature were discussed using the Cole-Cole plot. The dielectric relaxation mechanism was explained of both $\varepsilon'(\omega)$ and $\varepsilon''(\omega)$ at different frequencies and was found that it has temperature dependence.

References

[1] S. W. Martin, Ionic Conduction in Phosphate Glasses, J. Non-Cryst. Solid State Inorg. Chem. 28 (1991)163 205.https://doi.org/10.1111/j.1151-2916.1991.tb07788.x

[2] R. K. Brow, the structure of simple phosphate glasses, J. Non-Cryst. Solids 263-264 (2000) 1-28.https://doi.org/10.1016/S0022-3093(99)00620-1

[3] Yahia H. Elbashar, Ali M. Badr, Haron A. Elshaikh, Ahmed G. Mostafa, Ali M. Ibrahim, Dielectric and optical properties of CuO containing sodium zinc phosphate glasses, Processing and Application of ceramics 10 (4) (2016) 277-286.http://www.doiserbia.nb.rs/Article.aspx?id=1820-61311604277E

[4] D. D. Ramteke, R. E. Kroon, H. C. Swart, Infrared emission spectroscopy and upconversion of $ZnO\text{-}Li_2O\text{-}Na_2O\text{-}P_2O_5$ glasses doped with Nd^{3+} ions, J. Non-Cryst. Solids 457 (2017) 157-163.https://doi.org/10.1016/j.jnoncrysol.2016.12.006

[5] Dongemi SHI, YinggangZHAO,Spectroscopic properties and energy transfer of Nd^{3+}/Ho^{3+}-doped $Ga_2O_3\text{-}GeO_2$ glass by codoping Yb^{3+} ion, J. Rare Earths 34 (4) (2016) 368-373.https://doi.org/10.1016/S1002-0721(16)60035-2

[6] C.E. Smith, R. K. Brow, The properties and structure of zinc magnesium phosphate glasses, J. Non-Cryst. Solids 390 (2014) 51-58.https://doi.org/10.1016/j.jnoncrysol.2014.02.010

[7] K. Aida, T. Komatsu, V. Dimitrov, Thermalstability, electronic polarisability and optical basicity of ternary tellurite glasses, Phys. Chem. Glasses 42 (2) (2001) 103-111.

[8] ArnaudQuintas, Daniel Caurant, OdileMajérus, Pascal Loiseau, ThibaultCharpentier, Jean-LucDussossoy,ZrO_2 addition in soda-lime aluminoborosilicate glasses containing rare earths: Impact on rare earths environment and crystallization, J. Alloys Compd. 719 (2017)383-391.https://doi.org/10.1016/j.jallcom.2017.05.211

[9] L. Vijayalakshmi, K. Naveen Kumar, G.Bhaskar Kumar, Pyung Hwang, J. Non-Cryst. Solids, 475 (2017) 28-37.https://doi.org/10.1016/j.jnoncrysol.2017.08.024

[10] V. C. VeerannaGowda, Effect of Bi^{3+} ions on physical, thermal, spectroscopic and optical properties of Nd^{3+} doped sodium diborate glasses,Phys. B. 426 (2013) 58-64.https://doi.org/10.1016/j.physb.2013.06.007

[11] M. Shwetha, B. Eraiah, Influence of Er^{3+} ions on the physical, structural, optical, and thermal properties of $ZnO\text{-}Li_2O\text{-}P_2O_5$ glasses, App. Phys. A (2019) 125-221.https://doi.org/10.1007/s00339-019-2775-6

[12] AkshathaWagh, Y. Raviprakash, VyasaUpadhyaya, SudhaD. Kamath, Composition dependent structural and optical properties of PbF_2– TeO_2–B_2O_3–Eu_2O_3 glasses, Spectrochim.Acta A 151 (2015) 696-706.https://doi.org/10.1016/j.saa.2015.07.016

[13] V. Dimitrov, T. Komatsu, An interpretation of optical properties of oxides and oxide glasses in terms of the electronic ion polarizability and average single bond strength (review), J. Univ. Chem. Technol. Metall. 45 (2010) 219-250.

[14] Xinyu Zhao, Xiaoli Wang, Hai Lin, Zhiqiang Wang, Electronic polarizability and optical basicity of lanthanide oxides, Phys. B 392 (2007) 132-136.https://doi.org/10.1016/j.physb.2006.11.015

[15] El SayedYousef, M.M. Elokr, Y.M. AbouDeif, Optical, elastic properties and DTA of TNZP host tellurite glasses doped with Er^{3+}ions, J. Mol. Struct. 1108 (2016) 257–262.https://doi.org/10.1016/j.molstruc.2015.11.066

[16] F. Wang, Q.L. Liao, Y.Y. Dai, H.Z. Zhu, Properties and vibrational spectra of iron borophosphate glasses/glass-ceramics containing lanthanum, Mater. Chem. Phys. 166 (C) (2015) 215-222.https://doi.org/10.1016/j.matchemphys.2015.10.005

[17] Haijian Li, Xiaofeng Liang, Cuiling Wang, Huijun Yu, Zhen Li, Shiyuan Yang, Influence of rare earth addition on the thermal and structural stability of $CaO\text{-}Fe_2O_3\text{-}P_2O_5$ glasses, J. Mol. Struct. 1076 (2014) 592-599.https://doi.org/10.1016/j.molstruc.2014.08.032

[18] Yanling Liu, Feng Song, GuozhiJia, Y. Zhang, Yanbang Zhang, Yi Tang, Strong emission in Yb^{3+}/Er^{3+} co-doped phosphate glass ceramics, Results in Physics 7 (2017) 1987-1992.https://doi.org/10.1016/j.rinp.2017.06.023

[19] ParamjyotKumarJha, O. P. Pandey, K. Singh, Structure and crystallization kinetics of Li_2O modified sodium-phosphate glasses, J. Mol. Struct. 1094 (2015) 174-182.https://doi.org/10.1016/j.molstruc.2015.03.066

[20] C. Dayanand, G. Bhikshamaiah, V. Jaya Tyagaraju, M. Salagram, A.S.R. Krishna Murthy, Structural investigations of phosphate glasses: a detailed infrared study of the $x(PbO)\text{-}(1-x)\ P_2O_5$ vitreous system, J.Mater. Sci. Lett. 31 (1996) 1945-1967.

[21] Y. M. Lai, X. F. Liang, S. Y. Yang, J. X. Wang, L. H. Cao, B. Dai, Raman and FTIR spectra of iron phosphate glasses containing cerium, J. Mol. Struct. 992 (1-3) (2011) 84-88.https://doi.org/10.1016/j.molstruc.2011.02.049

[22] G.V. Rao, H. D. Shashikala, Structural, optical and mechanical properties of ternary CaO-CaF_2-P_2O_5 glasses, J. Adv. Ceram. 3(2) (2014) 109-116.

[23] Ray L. Frost, Yunfei Xi, Ricardo Scholz, Fernanda Maria Belotti, Mauro CândidoFilho, Infrared and Raman Spectroscopic Characterization of the Phosphate Mineral Leucophosphite $K(Fe^{3+})_2(PO_4)_2(OH) \cdot 2(H_2O)$, Spect. Lett. 46 (2013) 415-420.https://doi.org/10.1080/00387010.2012.733478

[24] Yoshiaki Tsunawaki, Analysis of CaO-SiO_2 AND CaO-SiO_2-CaF_2 glasses by Raman Spectroscopy, J. Non-Cryst. 44 (1981) 369-378.https://doi.org/10.1016/0022-3093(81)90039-9

[25] S. M. Abo-Naf, M. S. El-Amiry, A. A. Abdel-Khalek, FT-IR and UV–Vis optical absorption spectra of γ-irradiated calcium phosphate glasses doped with Cr_2O_3, V_2O_5 and Fe_2O_3, Opt. Mater. 30 (6) (2008) 900-909.https://doi.org/10.1016/j.optmat.2007.03.013

[26] F. H. Elbatal, Gamma ray interaction with copper-doped sodium phosphate glasses, J. Mater. Sci. 43 (3) (2008) 1070-1079.

[27] F. H. Elbatal, M. A. Marzouk, A. M. Abdelghany, UV–visible and infrared absorption spectra of gamma irradiated V_2O_5-doped in sodium phosphate, lead phosphate, zinc phosphate glasses: A comparative study, J. Non-Cryst. Solids 357 (3) (2011) 1027-1036.https://doi.org/10.1016/j.jnoncrysol.2010.11.040

[28] N. SoorajHussain, M.A. Lopes, J. D. Santos, A comparative study of CaO–P_2O_5–SiO_2 gels prepared by a sol–gel method, Mater. Chem. Phys. 88 (1) (2004) 5-8. https://doi.org/10.1016/j.matchemphys.2004.06.015

[29] J.I. Pankove, Optical Processes in Semiconductors, New Jersey, Prentice-Hall, 1971.

[30] J. Tauc, Amorphous and Liquid Semiconductors, New York: Plenum Ch. 4, 1974.

[31] A.F. Qasrawi, Refractive index, band gap and oscillator parameters of amorphous GaSe thin films, Cryst. Res. Technol., 40 (6) (2005) 610-614.https://doi.org/10.1002/crat.200410391

[32] F. Yakuphanoglu, M. Arslan, The fundamental absorption edge and optical constants of some charge transfer compounds. Opt. Mater. 27 (1) (2004)29–37.https://doi.org/10.1016/j.optmat.2004.01.017

[33] P. Chimalawong, J. Kaewkhao, C. Kedkaew, P. Limsuwan, Optical and electronic polarizability investigation of Nd^{3+}-doped soda-lime silicate glasses. J. Phys. Chem. Solids 71 (7) (2010)965–970.https://doi.org/10.1016/j.jpcs.2010.03.044

[34] S.S. Rao, G. Ramadevudu, M. Shareefuddin, A. Hameed, M.N. Chary, M.L. Rao, Optical properties of alkaline earth borate glasses. Int. J. Eng. Sci. Technol. 4 (2012)25–35.

[35] Pankove, J I 1975 Optical Processes in Semiconductors (NewYork: Dover) p 91.

[36] M. J. Miah, A. K. M. AktherHossain, Magnetic, Dielectric and Complex Impedance Properties of $xBa_{0.95}Sr_{0.05}TiO_3$–$(1 - x)BiFe_{0.9}Gd_{0.1}O_3$Multiferroic Ceramics, Acta Metall. Sin. (Engl. Lett.) 29 (6) (2016) 505-517.

[37] D. P. Almond, C. C. Hunter, A. R. West, The extraction of ionic conductivities and hopping rates from a.c. conductivity data, J. Mater. Sci. 19 (10) (1984)3236-3248.

[38] M. E. Sayed, M. M. Elokr , L. I. Soliman , H. A. Zayed, Synthesis and characterization of Li_2O modified sodium phosphate glasses, J. Sci. Res. Sci. 35 (2018) 417- 437. https://doi.org/10.21608/jsrs.2018.25524

[39] G.E. Pike, ac Conductivity of Scandium Oxide and a New Hopping Model for Conductivity, Phys. Rev. B6 (1972) 157.https://doi.org/10.1103/PhysRevB.6.1572

[40] D. Değer, K. Ulutas, Conduction and dielectric polarization in Se thin films, Vacuum 72 (3) (2003) 307-312.https://doi.org/10.1016/j.vacuum.2003.08.008

[41] R.H. Chen, Chen-Chen Yen, C.S. Shern,T.Fukami, Impedance spectroscopy and dielectric analysis in KH_2PO_4 single crystal, Solid State Ionics 177 (33-34) (2006) 2857-2864.https://doi.org/10.1016/j.ssi.2006.05.053

[42] Sh. A. Mansour, I. S. Yahia, G. B. Sakr, Electrical conductivity and dielectric relaxation behavior of fluorescein sodium salt (FSS), Solid State Communications 150 (29-30) (2010) 1386-1391.https://doi.org/10.1016/j.ssc.2010.04.029

[43] E.Abd El-Wahabb, M.M. Abd El-Aziz,E.R. Sharaf, M.A. Afifi, AC conductivity and dielectric properties of GeSexTl0.3 amorphous thin films, J. Alloys Compd.s 509 (34) (2011) 8595-8600.https://doi.org/10.1016/j.jallcom.2011.06.038